Bioactive Materials 25 (2023) 472–484

Contents lists available at ScienceDirect

Bioactive Materials

journal homepage: www.keaipublishing.com/en/journals/bioactive-materials

Apoptotic vesicles ameliorate lupus and arthritis via phosphatidylserine-mediated modulation of T cell receptor signaling

Runci Wang [a,b,c,d,*,1], Meng Hao [e,1], Xiaoxing Kou [b,e], Bingdong Sui [b], Maria Laura Sanmillan [f], Xiao Zhang [b], Dawei Liu [b], Jun Tian [b], Wenjing Yu [b], Chider Chen [b], Ruili Yang [b], Lingyun Sun [g], Yi Liu [c], Claudio Giraudo [f], Deepak A. Rao [d], Nan Shen [a], Songtao Shi [b,e,**]

[a] Shanghai Institute of Rheumatology/Department of Rheumatology, Renji Hospital, Shanghai Jiao Tong University School of Medicine, Shanghai, 200002, China
[b] Department of Anatomy and Cell Biology, School of Dental Medicine, University of Pennsylvania, Philadelphia, PA, 19104, USA
[c] Department of Rheumatology and Immunology, West China Hospital, Sichuan University, Chengdu, Sichuan, 610000, China
[d] Division of Rheumatology, Inflammation and Immunity, Brigham and Women's Hospital and Harvard Medical School, Boston, MA, 02105, USA
[e] South China Center of Craniofacial Stem Cell Research, Hospital of Stomatology, Guanghua School of Stomatology, Sun Yat-sen University, Guangzhou, Guangdong, 510080, China
[f] Department of Microbiology and Immunology, Sidney Kimmel Medical College, Thomas Jefferson University, Philadelphia, PA, 19107, USA
[g] Department of Rheumatology and Immunology, The Affiliated Drum Tower Hospital of Nanjing University Medical School, Nanjing, Jiangsu, 210008, China

ARTICLE INFO

Keywords:
Autoimmunity
T cell
MSC
Apoptosis
Extracellular vesicles

ABSTRACT

Mesenchymal stem cells (MSCs) influence T cells in health, disease and therapy through messengers of intercellular communication including extracellular vesicles (EVs). Apoptosis is a mode of cell death that tends to promote immune tolerance, and a large number of apoptotic vesicles (apoVs) are generated from MSCs during apoptosis. In an effort to characterize these apoVs and explore their immunomodulatory potential, here we show that after replenishing them systemically, the apoV deficiency in *Fas* mutant mice and pathological lymphoproliferation were rescued, leading to the amelioration of inflammation and lupus activity. ApoVs directly interacted with $CD4^+$ T cells and inhibited CD25 expression and IL-2 production in a dose-dependent manner. A broad range of Th1/2/17 subsets and cytokines including IFNγ, IL17A and IL-10 were suppressed while $Foxp3^+$ cells were maintained. Mechanistically, exposed phosphatidylserine (PtdSer/PS) on apoVs mediated the interaction with T cells to disrupt proximal T cell receptor signaling transduction. Remarkably, administration of apoVs prevented Th17 differentiation and memory formation, and ameliorated inflammation and joint erosion in murine arthritis. Collectively, our findings unveil a previously unrecognized crosstalk between MSC apoVs and $CD4^+$ T cells and suggest a promising therapeutic use of apoVs for autoimmune diseases.

1. Introduction

Stromal cells influence immune cells in the microenvironment through lines of intercellular communication including cell-cell contact, soluble factors, and a more recently discovered mechanism, extracellular vesicles (EVs) [1–3]. One example of stromal – immune cell interaction is the crosstalk between mesenchymal stem cells (MSCs) and T cells. Multipotent MSCs shape the stromal tissue, and their remarkable immunomodulatory capacity is widely applied in treating autoimmune disorders, such as systemic lupus erythematosus (SLE) [4] and rheumatoid arthritis (RA) [5]. Accumulation of activated T cells facilitates the breaching of tolerance and pathogenesis of these diseases; MSC therapy (MSCT) is effective in rescuing these T cell dysregulations in SLE and RA [6,7]. Intriguingly, the immunomodulation following MSCT can last for months after administration, despite that intact MSCs become undetectable within days [8,9]. Both living and apoptotic MSCs are

Peer review under responsibility of KeAi Communications Co., Ltd.
* Corresponding author. Shanghai Institute of Rheumatology/Department of Rheumatology, Renji Hospital, Shanghai Jiaotong University School of Medicine, 145 Middle Shandong Rd, Shanghai, 200002, China.
** Corresponding author. South China Center of Craniofacial Stem Cell Research, Hospital of Stomatology, Guanghua school of Stomatology, Sun Yat-sen University 74 Zhongshan 2Rd, Guangzhou, Guangdong, 510080, China.
E-mail addresses: runci.wang@gmail.com (R. Wang), shisongtao@mail.sysu.edu.cn (S. Shi).
[1] Co-first authors.

https://doi.org/10.1016/j.bioactmat.2022.07.026
Received 27 April 2022; Received in revised form 15 July 2022; Accepted 27 July 2022
Available online 9 August 2022

effective in inducing immune tolerance [10,11]. It remains unclear how dying MSCs achieve lasting immunomodulation and deciphering this form of stromal – immune interaction is critical to unlock the therapeutic potential of MSCs on autoimmunity.

Apoptosis is the most common form of cell death, occurring in billions of cells daily. Through a characteristic process of membrane blebbing and cellular component degradation, apoptotic cells break down and release numerous EVs. These subcellular structures, originally termed apoptotic bodies, turn out to be more diverse in their size, content and mechanism of formation than initially thought, and the term "apoVs" is now used to describe them. We have systemically characterized MSC-derived apoVs [12] and found an alternative route to eliminate apoVs *in vivo* [13]. ApoVs have advantages in intercellular communication since they can release multiple components inherited from parent cells either directly contact of living cells or endocosed by recipient cells to achieve therapeutic effect [14]. We previously identified that MSC-derived apoptotic bodies transferred proteins and microRNAs to recipient MSCs and rescued osteoporosis in apoptosis-deficient mice [15], improved type 2 diabetes via restoring liver macrophage homeostasis [16] and attenuated sepsis by switching neutrophil NETosis to apoptosis [17].

Apoptosis is the gatekeeper to immune tolerance by selecting T cell maturation in the thymus as well as controlling T cell activation in peripheral tissues [18]. Apoptosis is generally considered non-inflammatory as opposed to the inflammatory response triggered by necrosis. A number of recent studies have revealed promising immunosuppressive efficacy using apoptotic MSCs or mononuclear cells for treating inflammatory arthritis, graft-versus-host disease and sepsis [19,20]. To elucidate whether immune dysregulation and autoimmunity can be modulated with mesenchymal apoVs in this study, we characterized MSC apoVs and utilized *in vitro* cultured T cells and murine models of SLE and RA to study MSC apoV – T cell interaction.

2. Results

2.1. MSC apoVs rescue lymphoproliferation in mice with lupus

In this study, apoVs were mainly induced and collected from murine bone marrow mesenchymal stromal cells (BMMSCs) (Fig. S1A). As the first identified and well-studied MSCs, BMMSCs were used as cell source to generate apoVs. Apoptosis was induced with staurosporine (STS) via both caspase-dependent and caspase-independent pathways [21]. Using a modified method (Fig. S1B) based on our previous work [15], we identified new characteristics of apoVs. Compared to the non-apoptotic control, STS treatment increased the yield of EVs by greater than 5-fold (Figs. S1C–E), granting a quantitative advantage to apoVs over non-apoptotic EVs. The apoVs we isolated were smaller in size (100–350 nm in diameter, averaging 200 nm), with a spherical shape, and positive for the apoptosis marker PtdSer/PS (Figs. S1F–H). There were almost 10-fold as many of them as non-apoptotic BMMSC-derived exosomes from the same number of cells. ApoVs with similar characteristics can be isolated from the spleen (Fig. S1I) and the serum as well (Fig. S1J).

We hypothesized that the production of apoVs was proportionate to the level of apoptosis, translatable to the number of apoptotic cells when studied in a given cell culture system. With a defective apoptotic pathway, we found a decreased production of apoVs *in vitro* by *Fas*-mutant MRL/*lpr* BMMSCs (Figs. S2A and B) compared to the apoVs produced by the same number of BMMSCs from wild-type (WT) mice, suggesting an apoV deficiency relative to the number of cells in culture from MRL/*lpr* donors, which was restored by STS treatment. We also found that BMMSCs produced 245-fold more apoVs than an equal number of T cells *in vitro* (Fig. S2C), making BMMSCs a superior donor source of applicable apoVs.

To investigate whether there is an apoV deficiency *in vivo* similar to that *in vitro* in MRL/*lpr* mice, and to determine its relationship with T cells, we examined the levels of apoVs in age-matched female MRL/MpJ (MRL/wt), MRL/*lpr,* and MRL/*lpr* mice supplemented with weekly apoVs (derived from C57bl6 BMMSCs) for 4 weeks (Fig. 1A). In order to proportionately quantify apoVs relative to the number of cells *in vivo*, considering the great number of T cells accumulated in MRL/*lpr* mice compared to MRL/wt mice, a normalized ratio of apoV/T cell was used. We found an apoV deficiency relative to the T cell numbers in the circulation and spleen of MRL/*lpr* mice compared to MRL/wt mice, which was restored by apoV supplementation (Fig. 1B). ApoV replenishment significantly decreased the number of T cells accumulated in lymphoid tissues, such as the spleen and the mesenteric lymph node (MLN) (Fig. 1C). MRL/*lpr* mice had a 3-fold expansion of the $CD4^+$ T effector memory population (Tem) and a 6-fold reduction in the naïve $CD4^+$ T cell population comparing to MRL/wt mice, both of which were partially rescued by apoV replenishment (Fig. 1D and E). Inflammatory features including increased frequency of $IFN\gamma^+CD4^+$ T cells (Fig. 1F), increased serum IFNγ level (Fig. 1G), and decreased frequency of $Foxp3^+CD4^+$ T cells (Fig. 1H) were reversed in apoV-treated MRL/*lpr* mice. We next evaluated the long-term effect of apoV supplementation (Fig. 1I). Beneficial effects on preventing the development of severe proteinuria (Fig. 1J) and lupus nephritis (Fig. 1K) were observed with apoV replenishment. Long-term apoV supplementation greatly diminished the lymphoproliferation phenotype in MRL/*lpr* mice, as evidenced by dramatic reduction in the size and weight of the spleen and the MLN (Fig. 1L and M), which were accompanied by decreased T cell accumulation in the lung and the colon (Fig. 1N). The level of anti-dsDNA IgG was also decreased in the long-term apoV supplementation group (Fig. 1O). Of further importance, these beneficial effects on T cells, tissues, and serological parameters were reflected in the prolonged survival of apoV-supplemented mice with lupus (Fig. 1P). These data suggest that there is an association between the quantity of apoVs and T cells, and that BMMSC-derived apoVs are therapeutically beneficial for murine lupus.

2.2. ApoVs exert a unique immunomodulatory function via tuning the activity of $CD4^+$ T cells

To investigate whether the effect of apoVs on $CD4^+$ T cells is beneficial beyond *Fas*-mutant MRL/*lpr* mice, we expanded T cells from splenocytes of C57BL/6 mice. Firstly, by controlling the input apoV number with respect to splenocytes, we compared the dose-effect of apoVs on the activation of $CD4^+$ T cells (Fig. 2A). While the expansion of $CD25^+$ activated $CD4^+$ T cells gradually decreased as the dosage of apoVs increased in splenocyte culture stimulated with anti-CD3/CD28 antibodies, it remained steady in unstimulated culture regardless of the dosages of apoVs. This suppressive effect reached a plateau with an apoV: splenocyte ratio of 0.2 : 1 or higher (Fig. 2A and B). IL-2 in the supernatant responded with a dose-dependent decrease inversely proportional to the number of apoVs in the culture (Fig. 2C). Next, we examined whether the effect of apoVs on T cells would be dampened by stronger stimulation on the T cell receptor. Contrary to our expectation, fewer activated $CD4^+$ T cells were found in splenocytes stimulated with a higher concentration of anti-CD3/CD28 antibodies when apoVs were present (Fig. 2D). When apoVs were present during non-polarizing stimulation with anti-CD3/CD28 antibodies, expansion of effector populations including Th1 ($IFN\gamma^+CD4^+$), Th17 ($IL\text{-}17A^+CD4^+$) and Th2 ($IL\text{-}4^+CD4^+$) were all limited, accompanied by a decreased level of supernatant cytokines including IFNγ, IL-17A and IL-10 (Fig. 2E and F). In contrast to the increased $Foxp3^+$ frequency we observed in MRL/*lpr* mice supplemented with apoVs, $Foxp3^+CD4^+$ T cells *in vitro* were neither expanded when apoVs were present, nor significantly suppressed like other effector subsets (Fig. 2G). Our findings demonstrated that apoVs possess a unique immunomodulatory function that results in dose-dependent, preferential suppression of effector $CD4^+$ T cells. This function appears to be involved in the maintenance of immune homeostasis, as this modulatory effect of apoVs was minimal on unstimulated T cells and amplified when T cells had stronger TCR

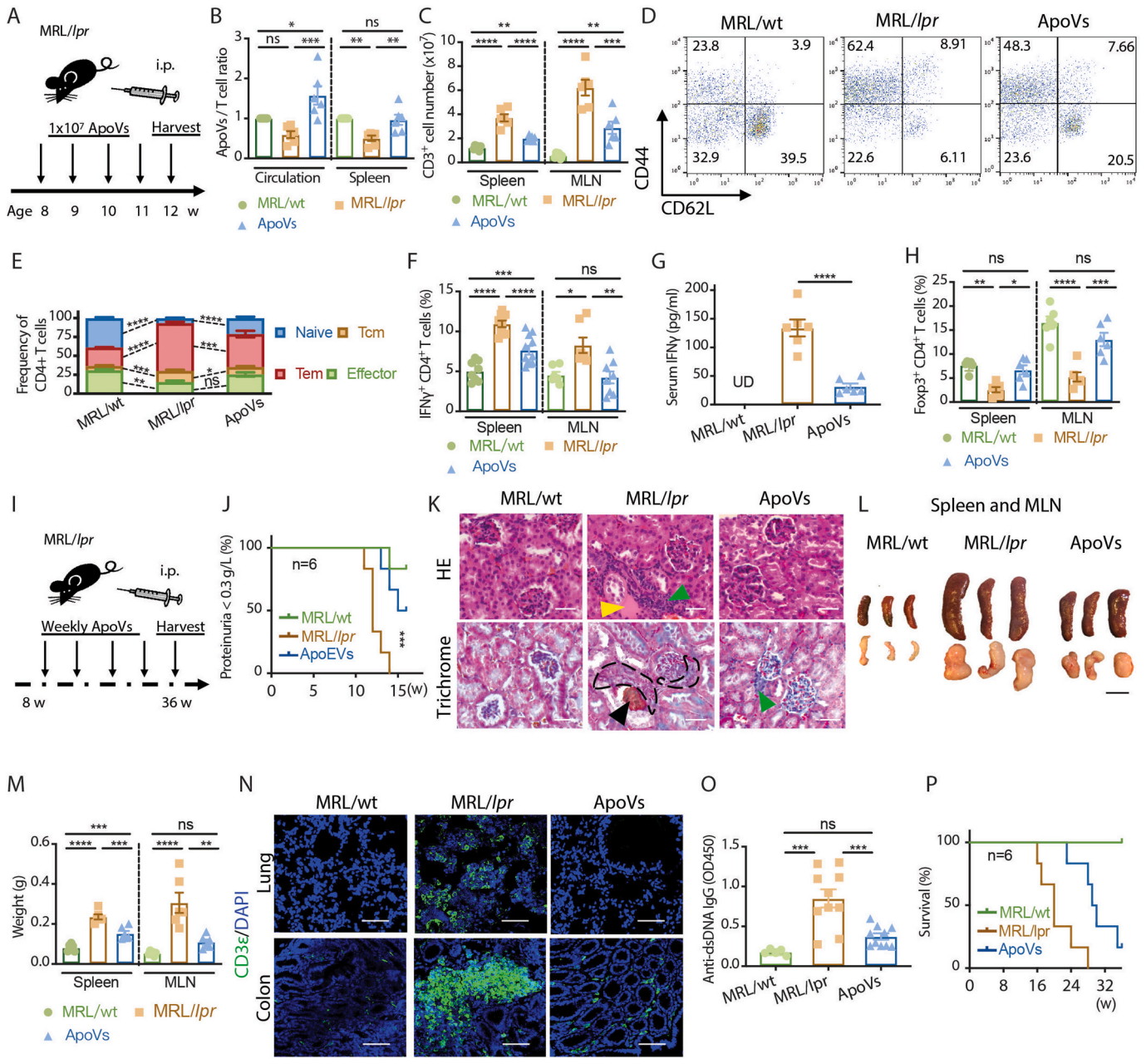

Fig. 1. ApoVs rescue dysregulated T cell proliferation and ameliorate murine lupus. (A) Scheme of 4-week systemic apoV supplementation in MRL/*lpr* mice. **(B)** Normalized ratio of apoVs/T cells in circulation and spleen of MRL/*lpr* mice treated with or without apoVs for 4 weeks in comparison to age-matched MRL/*wt* mice analyzed by flow cytometry. N = 6 per group. **(C)** Numbers of $CD3^+$ cells in spleen and mesenteric lymph node (MLN) of MRL/*lpr* mice treated with or without apoVs for 4 weeks in comparison to age-matched MRL/*wt*. N = 6 per group. **(D, E)** Frequency of naïve, central memory (Tcm), effector memory (Tem), and effector $CD4^+$ T cells in spleen of MRL/*lpr* mice treated with or without apoVs for 4 weeks in comparison to age-matched MRL/*wt*. N = 6 per group. **(F, G)** Frequency of $IFN\gamma^+CD4^+$ T cells in spleen and MLN analyzed by flow cytometry, and serum levels of IFNγ measured by ELISA of MRL/*lpr* mice treated with or without apoVs for 4 weeks in comparison to age-matched MRL/*wt*. N = 6–11 per group. **(H)** Frequency of $Foxp3^+CD4^+$ T cells in spleen and MLN of MRL/*lpr* mice treated with or without apoVs for 4 weeks in comparison to age-matched MRL/*wt*. N = 6 per group. **(I)** Scheme of long-term systemic apoV supplementation in MRL/*lpr* mice. **(J)** Severe proteinuria (>0.3 g/L) onset in MRL/*lpr* mice treated with or without apoVs for 8 weeks in comparison to age-matched MRL/*wt* mice. N = 6 per group. **(K)** Representative hematoxylin and eosin (HE) staining and Masson's trichrome staining of kidney from MRL/*lpr* mice treated with or without apoVs for 12 weeks in comparison to age-matched MRL/*wt* mice. Green triangle indicates immune cell infiltration. Yellow triangle indicates eosinophilic material deposition. Black triangle indicates necrotic glomerulus. Black contour indicates crescent formation. Scale bar = 50 μm. **(L, M)** Size and weight of spleen and MLN of MRL/*lpr* mice treated with or without apoVs for 12 weeks in comparison to age-matched MRL/*wt* mice. N = 6 per group. Scale bar = 1 cm. **(N)** Representative immunofluorescence staining of $CD3^+$ T cells in lung and colon of MRL/*lpr* mice treated with or without apoVs for 12 weeks in comparison to age-matched MRL/*wt* mice. Scale bar = 200 μm. **(O)** Serum levels of anti-dsDNA IgG measured by ELISA from MRL/*lpr* mice treated with or without apoVs for 4 weeks in comparison to age-matched MRL/*wt*. N = 5–15 per group. **(P)** Survival of MRL/*lpr* mice treated with or without apoVs starting at 8 weeks in comparison to age-matched MRL/*wt* mice. N = 6 per group. Kruskal-Wallis test and ANOVA was used for comparison among three groups when appropriate. Mantel-Cox test was used for proteinuria and survival analysis. Data are shown as mean ± standard deviation. ns, not significant. *, $p < 0.05$. **, $p < 0.01$. ***, $p < 0.001$. ****, $p < 0.0001$.

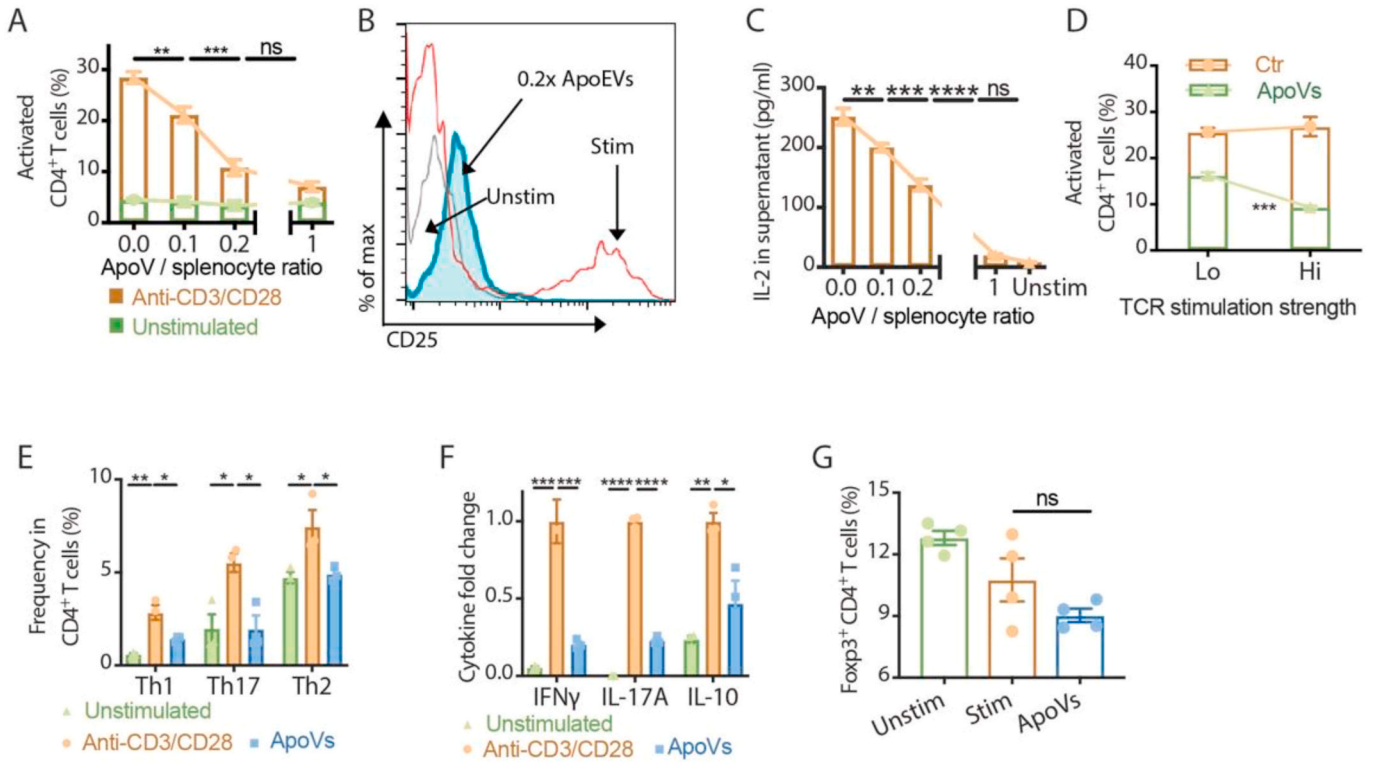

Fig. 2. ApoVs preferentially suppress activation of effector T cells in a dose-dependent manner. (A, B) Frequency of activated $CD4^+$ T cells measured *in vitro* after 3 days with or without anti-CD3/CD28 antibody stimulation in the presence of different doses of apoVs. Representative flow cytometric analyses of CD25 expression on $CD4^+$ T cells are shown. N = 5 per group. **(C)** Level of IL-2 in splenocyte culture supernatants measured by ELISA after 3 days of anti-CD3/CD28 antibody stimulation in the presence of different doses of apoVs. N = 5 per group. **(D)** Frequency of activated $CD4^+$ T cells measured *in vitro* after 3 days with 1 μg/mL (Lo) or 10 μg/mL (Hi) anti-CD3/CD28 antibody stimulation in the presence of 0.2x apoVs. Representative flow cytometric analyses are shown. N = 3–4 per group. **(E)** Frequency of Th1, Th17 and Th2 of $CD4^+$ T cells measured *in vitro* after 3 days with or without anti-CD3/CD28 antibody stimulation in the presence of 0.2x apoVs. N = 3 per group. **(F)** Levels of IFNγ, IL-17A and IL-10 in splenocyte culture supernatants measured by ELISA after 3 days of anti-CD3/CD28 antibody stimulation in the presence of 0.2x apoV. N = 3 per group. **(G)** Frequency of $Foxp3^+CD4^+$ T cells measured *in vitro* after 3 days with or without anti-CD3/CD28 antibody stimulation in the presence of 0.2x apoVs. N = 4 per group. Mann-Whitney test and student's *t*-test was used for comparison between two groups when appropriate. Kruskal-Wallis test and ANOVA was used for comparison among multiple groups when appropriate.Data are shown as mean ± standard deviation. ns, not significant. *, $p < 0.05$. **, $p < 0.01$. ***, $p < 0.001$. ****, $p < 0.0001$.

stimulation.

To investigate the effect of apoVs on Fas-intact T cells *in vivo*, we administered weekly injections of apoVs to C57BL/6 mice for 4 weeks (Fig. S3A). The frequency of $CD25^+$ activated $CD4^+$ T cells transiently decreased at 24 h post-injection, more significantly in the spleen than in the circulation (Fig. S3B). Systemic apoV administration did not alter the homeostasis of C57bl6 mice, as shown by the comparable frequencies of effector-memory-naïve $CD4^+$ T cells (Fig. S3C), Th1/Th17/Th2 (Fig. S3D) and Treg (Fig. S3E) subsets. These data indicate that apoVs did not compromise the T cell immunity in healthy mice under physiological conditions.

2.3. ApoVs inhibit proximal TCR signaling via direct contact with T cells

To investigate if immunomodulation can be achieved via direct contact of apoVs with T cells, we investigated whether T cell activation can be suppressed in the absence of macrophages. After $CD11b^+$ cells were depleted in CD11b-DTR mice using diphtheria toxin (Fig. 3A), the frequency of $CD25^+$ activated $CD4^+$ T cells in the spleen also decreased at 24 h post-injection (Fig. 3B), suggestive of macrophage-independent effects. Then, when naïve $CD25^-CD4^+$ T cells were purified from mouse spleen and stimulated *in vitro*, apoVs were able to directly act on these T cells and greatly suppress their activation (Fig. 3C–E). As apoVs express the apoptotic marker PS on their membrane surface, to further elucidate how apoVs modulate T cells activity via direct contact, we attempted to block PS-based interaction using annexin V (A5) pre-treatment. A5-pretreatment successfully dampened the suppressive effect of apoVs on $CD4^+$ T cell activation and the IL-2 level (Fig. 3F and G).

We next compared the effects of apoVs, exosomes and conditioned medium containing soluble components of apoVs (sApoVs) prepared from the same number of BMMSCs (Fig. 3H). Activation of $CD4^+$ T cells was best suppressed by direct contact with apoVs, to a significantly lesser degree by the soluble components in apoV-conditioned-medium, and not at all by exosomes (Fig. 3I). Using equal numbers of apoVs derived from BMMSCs, C57bl6 (denoted as WT) T cells and MRL/*lpr* (denoted as LPR) T cells, once the doses of apoVs reached the suppression plateau we described before, comparable suppression of $CD4^+$ T cell activation was achieved regardless of the cell source, although it took a much larger number of T cells than BMMSCs to obtain the same number of apoVs (Fig. 3J). ApoVs were effective in suppressing activation of $CD4^+$ T cells in human peripheral blood mononuclear cells (PBMCs), indicating species-independent efficacy (Fig. 3K). These data confirm that the main functional molecules of apoVs are broadly expressed by different types of cells and on the membrane surface of apoVs to allow contact-mediated suppression of T cells.

To track the contact and interaction of apoVs with T cells, we performed time-course immunofluorescence tracking as well as live cell imaging of the apoV-T cell co-culture. Thirty to 60 min after adding apoVs to T cell culture, 40–60% of T cells co-localized with PKH26-labelled apoVs, indicating direct contact (Fig. 3L and M). Notably, when blocked with A5 pre-treatment, contact between apoVs and T cells drastically decreased (Fig. 3N). Moreover, in T cells treated with apoVs,

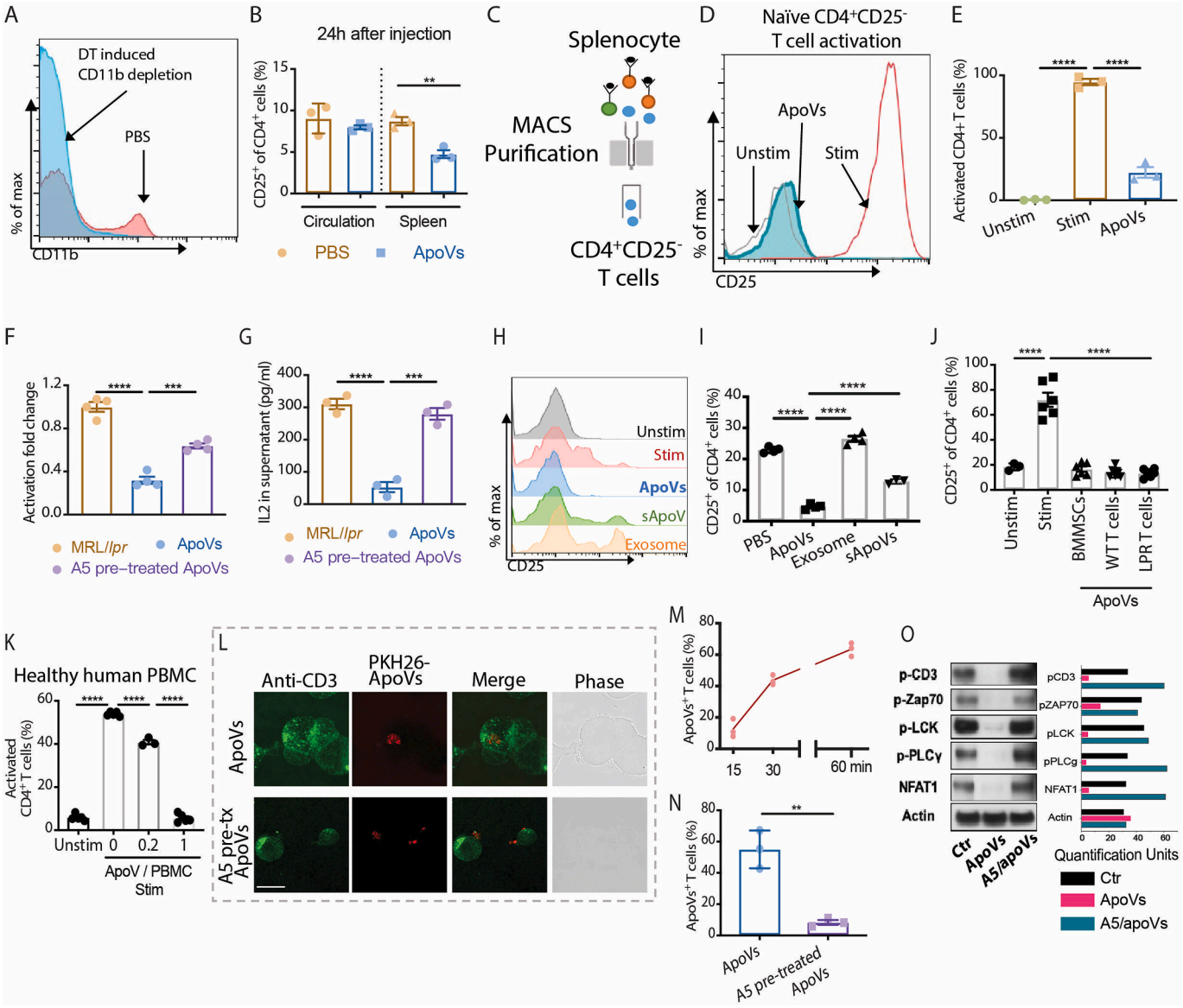

Fig. 3. ApoVs directly interact with T cells via phosphatidylserine to inhibit TCR signaling. (A) Representative images of flow cytometric analysis of CD11b expression on CD11b-DTR mice treated with or without diphtheria toxin (DT). **(B)** Frequency of $CD25^+CD4^+$ T cells in circulation and spleen of CD11b-DTR mice at 24 h after treatment with or without apoVs. N = 3 per group. **(C–E)** The experimental scheme, representative flow cytometric analyses and quantification of CD25 expression from naïve $CD4^+$ T cell cultures that were unstimulated (Unstim) or anti-CD3/CD28 stimulated with or without 0.2x apoVs. N = 3 per group. **(F)** Activation fold change of naïve $CD4^+$ T cells stimulated in the presence of PBS (Ctr), 0.2x apoVs (ApoVs) or 0.2x annexin V (A5) pre-treated apoVs. N = 4 per group. **(G)** IL-2 levels in supernatants of naïve $CD4^+$ T cells stimulated in the presence of PBS (Ctr), 0.2 x apoVs (ApoVs) or 0.2 x annexin V (A5) pre-treated apoVs. N = 4 per group. **(H, I)** Representative flow cytometric analyses and quantification of CD25 expression on $CD4^+$ T cells from splenocyte cultures that were unstimulated (Unstim), anti-CD3/CD28 stimulated in the presence of PBS (Stim), apoVs, exosome or soluble fraction of apoVs (sApoVs). N = 3–4 per group. **(J)** Frequency of $CD25^+CD4^+$ T cells measured *in vitro* after 3 days with or without anti-CD3/CD28 antibody stimulation in the presence of 1x apoV (1 apoV: 1 T cell) derived from BMMSCs or T cells from C57bl6 (WT) and MRL/*lpr* (LPR) mice. N = 3–6 per group. **(K)** Frequency of activated $CD4^+$ T cells in healthy human peripheral blood mononuclear cells (PBMC) measured *in vitro* after 3 days with or without anti-CD3/CD28 antibody stimulation in the presence of different doses of apoVs derived from mouse BMMSCs. N = 3–5 per group. **(L)** Representative immunofluorescence staining of $CD3^+$ T cells and PKH26-labelled apoVs with or without A5 pre-treatment. Scale bar = 10 μm. **(M)** Frequency of $apoVs^+$ T cells after 15, 30 and 60 min of coculture measured by immunofluorescence staining. N = 3 per group. **(N)** Frequency of $apoVs^+$ T cells after 60 min of coculture with or without A5 pre-treatment measured by immunofluorescence staining. N = 3 per group. **(O)** Western blotting shows expression of proximal TCR signaling proteins p-CD3, p-ZAP70, p-LCK, p-PLCγ and NFAT1 in naïve $CD4^+$ T cells stimulated with anti-CD3/CD28 antibodies in the presence of PBS (Ctr), 0.2 x apoVs (ApoVs) or 0.2 x annexin V (A5) pre-treated apoVs for 1 h. Mann-Whitney test and student's *t*-test was used for comparison between two groups when appropriate. Kruskal-Wallis test and ANOVA was used for comparison among three groups when appropriate. Data are shown as mean ± standard deviation. **, $p < 0.01$. ***, $p < 0.001$. ****, $p < 0.0001$.

the phosphorylation of proximal TCR signaling was diminished, showing a blockage of signaling transduction, which was rescued as a result of the decreased contact between A5-pretreated apoVs and T cells (Fig. 3O).

2.4. Exposed PS on apoVs is required for immunomodulation in murine lupus

We next test whether PS was indeed the key to apoV interaction with T cells. PS can be recognized by receptors such as T-cell immunoglobulin

and mucin-domain containing-3 (TIM-3), a coinhibitory receptor expressed on strongly or chronically stimulated T cells, particularly Th1 and Th17 cells [22]. Through confocal imaging of stimulated T cells, we found a colocalizing pattern of TIM-3 and the ganglioside GM-1-enriched lipid raft structure of the cell membrane, which indicates physical proximity between TIM-3 and the TCR complex (Fig. S4A). When PKH26-labelled apoVs were added to stimulated T cells, these apoVs also colocalized with GM-1 and appeared to be inserted into the lipid raft as well (Fig. S4B). ApoVs came into close contact with the CD3 molecule on the lipid raft (Fig. S4C), providing a physical base for apoVs to modulate CD3-TCR complex activity on T cells. When SDS-soluble lipid raft components were extracted from T cells, we confirmed TIM-3 expression on the caveolin-containing lipid raft, as well as CD3, but not other cytoplasmic proximal TCR signaling molecules such as Zap70 or LCK (Fig. S4D). Phosphorylation of CD3 was also diminished in T cells treated with apoVs, but not with A5-pretreated apoVs (Fig. S4D). In addition, by blocking T cells with TIM-3 antibody, the suppressive effect of apoVs on T cells was partially blocked (Fig. S4E), supporting the notion that the interaction between PS on apoVs and TIM-3 on T cells is important for the immunomodulatory function of apoVs.

To further confirm that blocking PS would suppress the immunomodulatory effect of apoVs on T cells *in vivo*, we gave MRL/*lpr* mice weekly supplements of apoVs or A5-pretreated apoVs for 4 weeks (Fig. 4A). A5-pretreated apoVs failed to correct the deficient level of apoVs with respect to T cells in the circulation and the spleen of these mice (Fig. 4B). Without a corrected apoV level, not surprisingly, A5-pretreated apoVs did not rescue the frequency of IFNγ$^+$CD4$^+$ T cells nor the serum IFNγ level (Fig. 4C and D) like normal apoVs did. A5-pretreated apoVs performed poorly at rescuing the expansion of CD4$^+$ Tem and the reduction of naïve CD4$^+$ T cells compared to normal apoVs (Fig. 4E and F), and similarly in rescuing the level of anti-dsDNA IgG (Fig. 4G). Taken together, these data suggest that apoVs ameliorate murine lupus via PS-based immunomodulation.

2.5. ApoVs render therapeutic benefits for inflammatory arthritis via PS

We next investigated whether apoVs can be applied therapeutically for another autoimmune disorder, collagen-induced arthritis in mice. Dysregulated Th17 cells play an important role in inflammatory arthritis [23]. We first examined whether apoVs could affect the differentiation of Th17 cells. Under Th17 polarizing conditions, we found a dose-dependent suppressive effect of apoVs on Th17 differentiation (Fig. S5A). A significant suppression of IL-17A production by apoVs was detected as early as 6 h of co-culture (Fig. S5B). Compared to their BMMSC source cells, which have been shown to suppress Th17 cells *in vitro* and *in vivo* [24], apoVs from the same number of BMMSCs had an even stronger suppressive effect on Th17 differentiation (Fig. S5C).

PKH26-labelled apoVs were mainly distributed in the liver and femur of MRL/*lpr* and arthritis mice (Fig. S6A and B). We also found that peripheral blood circulating vesicles contained apoVs which were decreased significantly after 7 days of apoV administration (Fig. S6C and D). Furthermore, intraperitoneally injected apoVs can remain in the liver and femur for 7 days (Fig. S6B) and do not cause any damage in these tested organs as shown by histological analysis (Fig. S6E and F).

We next compared the therapeutic benefit of apoVs to that of BMMSCs and TNF inhibitors (TNFi) in arthritic mice (Fig. 5A). We found lower arthritis clinical scores in mice receiving apoVs, BMMSCs or TNFi during the entire course of disease, with apoVs and TNFi outperforming BMMSCs from D33 to the endpoint (Fig. 5B and C). Tissue damage involving the bone and joint was evaluated with a histological scoring system based on the level of inflammation, pannus formation, as well as cartilage and bone erosion (Fig. 5D and E). The comprehensive

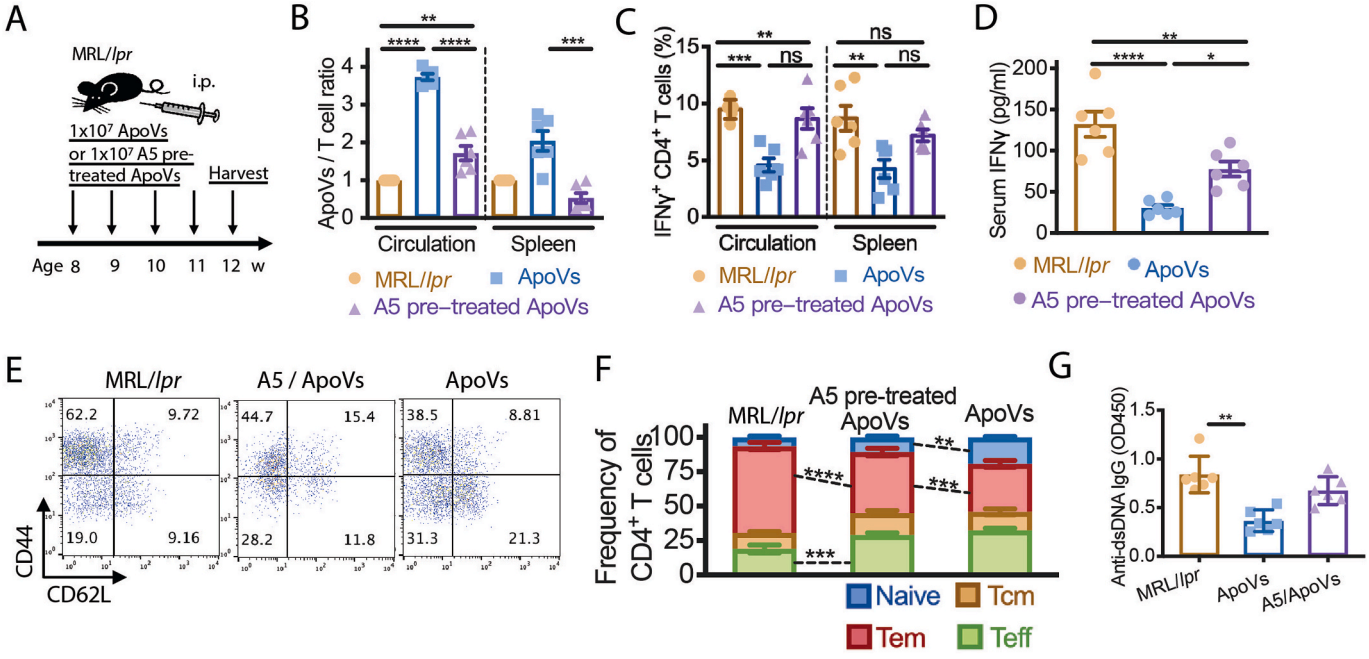

Fig. 4. Blocking phosphatidylserine on apoVs stunts their immunoregulatory effect in murine lupus. (A) Scheme of 4-week systemic infusion of apoVs or A5 pre-treated apoVs in MRL/*lpr* mice. **(B)** Normalized ratios of apoVs/T cells in circulation and spleen of MRL/*lpr* mice treated with apoVs or A5 pre-treated apoVs for 4 weeks in comparison with age-matched MRL/*lpr* mice analyzed by flow cytometry. N = 6 per group. **(C, D)** Frequency of IFNγ$^+$CD4$^+$ T cells in circulation and spleen analyzed by flow cytometry, and serum levels of IFNγ measured by ELISA of MRL/lpr mice treated with apoVs or A5 pre-treated apoVs for 4 weeks in comparison with age-matched MRL/*lpr* mice analyzed by flow cytometry. N = 6 per group. **(E, F)** Frequency of naïve, central memory (Tcm), effector memory (Tem), and effector CD4$^+$ T cells in spleen of MRL/*lpr* mice treated with apoVs or A5 pre-treated apoVs for 4 weeks in comparison with age-matched MRL/*lpr* mice. N = 4–6 per group. **(G)** Serum levels of anti-dsDNA IgG measured by ELISA from MRL/*lpr* mice treated with apoVs or A5 pre-treated apoVs for 4 weeks in comparison with age-matched MRL/*lpr* mice. N = 6 per group. Mann-Whitney test and student's *t*-test was used for comparison between two groups when appropriate. Kruskal-Wallis test and ANOVA was used for comparison among three groups when appropriate. Data are shown as mean ± standard deviation. ns, not significant. *, $p < 0.05$. **, $p < 0.01$. ***, $p < 0.001$. ****, $p < 0.0001$.

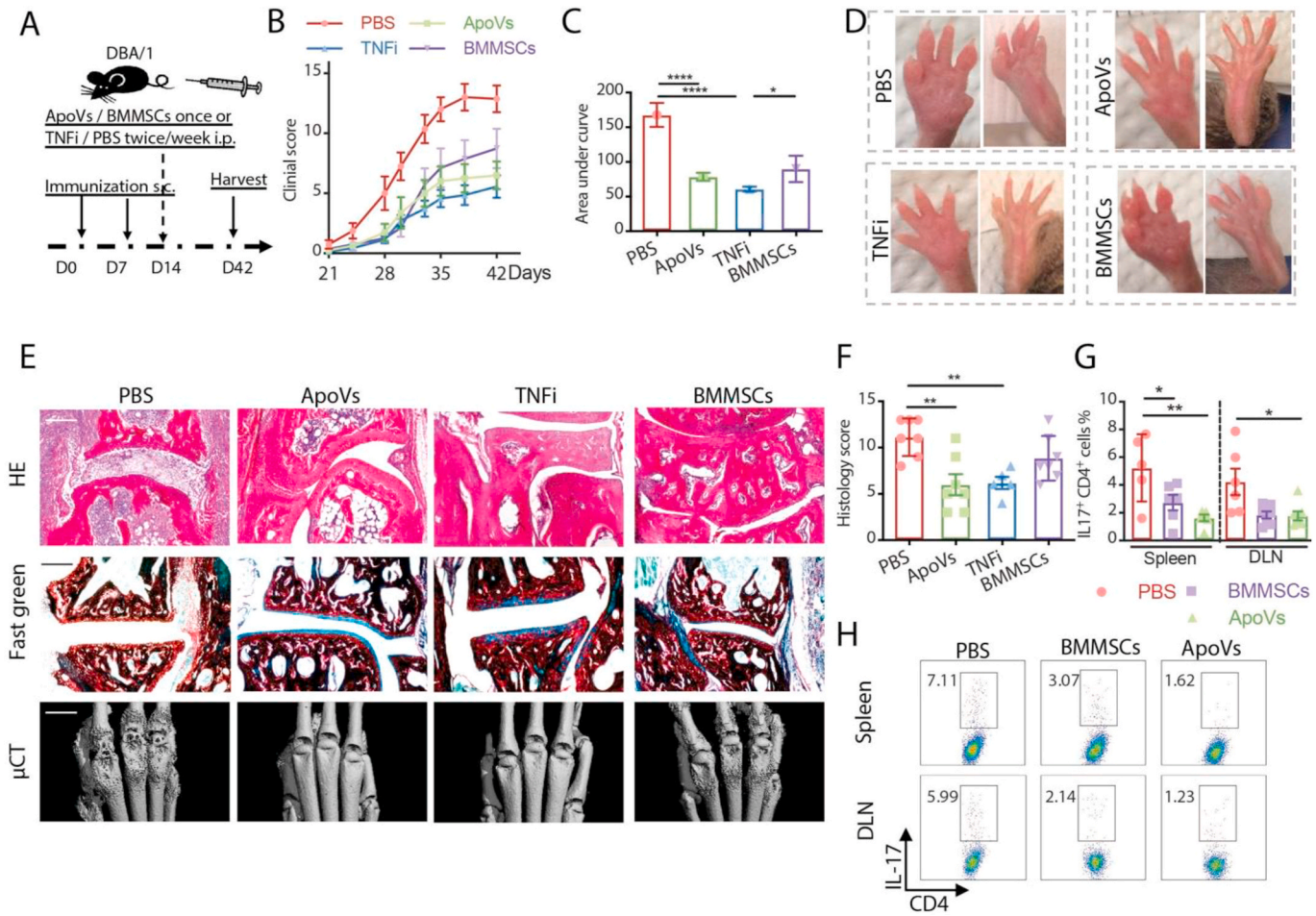

Fig. 5. One-time apoV injection ameliorates murine arthritis. (A) Scheme of D14 systemic apoV injection in collagen-induced arthritic DBA/1 (CIA) mice. **(B, C)** Comparison of clinical scores measured every 3 days in mice receiving D14 apoVs once, D14 BMMSCs once, or TNFi or PBS twice/week starting from D14 until the endpoint. N = 7–8 per group. **(D, F)** Representative images and histological scores of arthritic front and hind paws of CIA mice receiving apoVs, BMMSCs, TNFi or PBS at the time of harvest. **(E)** Representative images of HE staining, fast green staining of collagen (green) and microCT (μCT) of arthritic joints of CIA mice receiving apoVs, BMMSCs, TNFi or PBS at the time of harvest. N = 5–7 per group. Scale bar = 200 μm in HE and fast green staining. Scale bar = 1 mm in μCT images. **(G, H)** Representative flow cytometric staining of IL-17 and frequency of Th17 cells from DLN and spleen of CIA mice receiving apoVs, BMMSCs or PBS at the time of harvest. N = 5–7 per group. Kruskal-Wallis test and ANOVA was used for comparison among three groups when appropriate. Data are shown as mean ± standard deviation. *, $p < 0.05$. **, $p < 0.01$. ****, $p < 0.0001$.

histological scores showed that one infusion of apoVs led to significantly improved tissue integrity, similar to the impact of TNFi and outperforming that of BMMSCs (Fig. 5F). Mice treated with apoVs or BMMSCs showed a reduction in the frequency of Th17 cells in both their spleen and draining lymph nodes (DLN) compared to PBS-treated controls, while apoV administration resulted in an even lower level of Th17 cells in the spleen than BMMSCs did (Fig. 5G and H). These findings supported the notion that apoVs show outstanding therapeutic benefits for inflammatory arthritis.

Finally, we evaluated the role of PS in mediating the therapeutic effect of apoVs in arthritis. We added equal numbers of apoVs and liposomes made entirely of PS to T cells separately, and they exhibited comparable suppression of T cell activity *in vitro* (Fig. 6A), suggesting PS on apoVs could directly exert an immunomodulatory effect on T cells. ApoVs, A5-pretreated apoVs, PS liposomes or PBS were given once at the time of primary immunization (Fig. 6B), and arthritic activity was monitored in DBA/1 mice for 42 days. While mice treated with apoVs and PS liposomes showed a significantly milder clinical arthritic activity, mice that received A5 pre-treated apoVs had similarly severe arthritis to PBS-treated controls (Fig. 6C–E). When the frequency of Tem among $CD4^+$ T cells in the blood was measured at D14 and D42, apoV-treated mice had the lowest Tem at both time points (Fig. 6F). A decreased level of Th17 cells in DLN and the spleen was seen in apoV- and PS liposome-treated mice, but not in mice receiving A5-pretreated apoVs (Fig. 6G). Collectively, these data indicate that stroma-derived apoVs effectively modulate the activity of $CD4^+$ T cells via exposed PS and protect mice from developing inflammatory arthritis *in vivo*.

3. Discussion

In this study we showed that MSC-apoVs have the capacity to modulate T cell immunity and ameliorate autoimmune disorders. Phenotypically, supplementing mesenchymal apoVs partially rescued apoptosis-defective lymphoproliferation in MRL/*lpr* mice and attenuated disease severity in murine model of lupus and arthritis. Functionally, MSC-apoVs directly modulated T cell activity by suppressing effector T cell activation and IL-2 secretion in a dose-dependent manner. Mechanistically, direct membrane contact of apoVs and T cells mediated by PS disrupted CD3 phosphorylation on the lipid raft and destabilized T cell activation signal transduction. These results unveiled a previously unrecognized mechanism of apoV-mediated tuning of T cell membrane structure and TCR signaling, and a beneficial role of apoVs in regulating T cell activity in autoimmune disorders.

MSC therapy has demonstrated potent efficacy in treating various

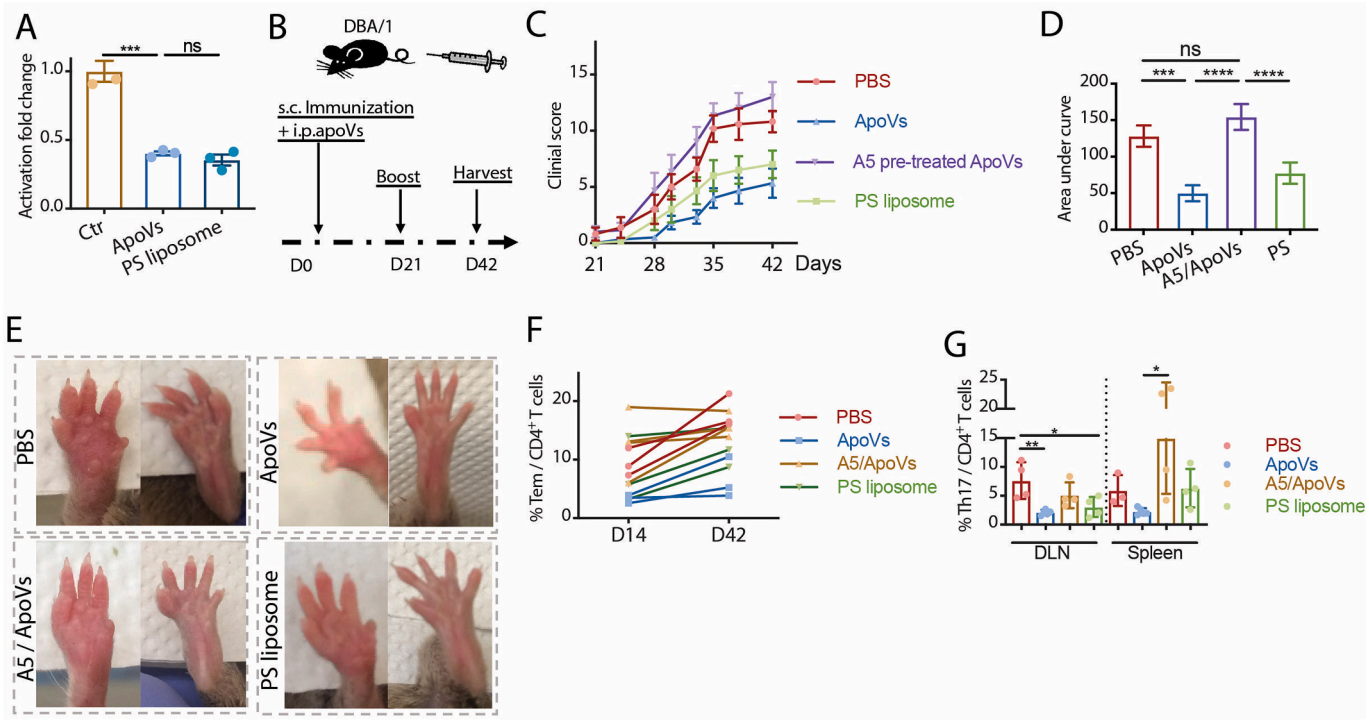

Fig. 6. ApoVs prevent T cell activation in murine arthritis *via* phosphatidylserine. (A) Activation fold change of naïve CD4$^+$ T cells stimulated in the presence of PBS (Ctr), 0.2 x apoVs (ApoVs) or 0.2 x phosphatidylserine (PS) liposomes. N = 3 per group. **(B)** Scheme of D0 systemic apoV injection in collagen-induced arthritic DBA/1 (CIA) mice. **(C, D)** Comparison of clinical scores in mice receiving D0 PBS, apoVs, A5 pre-treated apoVs, or PS liposomes measured every 3 days from D21 until the endpoint. N = 5–6 per group. **(E)** Representative images of arthritic front and hind paws of CIA mice receiving D0 PBS, apoVs, A5 pre-treated apoVs, or PS liposomes at the time of harvest. **(F)** Frequency of Tem CD4$^+$ T cells in circulation of CIA mice receiving D0 PBS, apoVs, A5 pre-treated apoVs, or PS liposomes at D14 and D42. N = 3–4 per group. **(G)** Frequency of Th17 cells from draining lymph nodes (DLN) and spleen of CIA mice receiving D0 PBS, apoVs, A5 pre-treated apoVs, or PS liposomes. N = 3–5 per group. Kruskal-Wallis test and ANOVA was used for comparison among three groups when appropriate. Data are shown as mean ± standard deviation. ns, not significant. *, $p < 0.05$. **, $p < 0.01$. ***, $p < 0.001$. ****, $p < 0.0001$.

inflammatory and autoimmune disorders [4,25] as one of the most popular platforms to produce anti-inflammatory factors including EVs [26–28]. Smaller in size and greater in number than their cells of origin, EVs are easily disseminated in the body fluid and tissue spaces, making them easily accessible to nanometer-scale molecular complexes (such as major histocompatibility and T cell receptor) on recipient cells [29]. Our results revealed intriguing features of the production of MSC-EVs: apoVs generated by MSCs overwhelmingly outnumber those generated by an equal amount of T cells, and EV levels significantly increase when MSCs undergo apoptosis. Given these advantages, it is not surprising that apoVs are critical players in MSC-mediated immunomodulation.

Dysregulations of T cells, including excessive lymphoproliferation [30], disproportionate expansion of pro-inflammatory CD4$^+$ subsets [31] and uncontrolled activation [32], are the gateways leading to autoimmunity. ApoVs showed robust suppressive effects in response to strong T cell activation in cell culture and in murine lupus and arthritis, while maintaining a basal level of immune activity with balanced CD4$^+$ T cell subsets in unstimulated cell culture and uninflammed mice, suggesting that apoV-mediated T cell modulation adapts to the extent of immune dysregulation. Through suppressing IL-2 secretion, apoVs showed preferential suppression of effector subsets including Th1 and Th17 cells, while the frequency of Tregs appeared to be less affected by IL-2 deprivation (possibly due to their higher affinity to IL-2), making apoVs suitable for treating inflammatory and autoimmune disorders. Besides the factors contributing to T cell accumulation such as proliferation and maturation, defective cell death may also lead to T cell accumulation, and these factors are not independent, as in some cases T cell activation may prevent apoptosis while in others activated T cells are more prone to death. Whether apoVs induce T cell death as an axillary mechanism to rescue aberrant T cell activation in autoimmune disorders remains to be elucidated.

In the context of tumors [33], viral infection [34] and autoimmune therapy [35], it is proposed that apoptotic cells pass on their immunomodulatory signals via cell-cell contact during efferocytosis by macrophages, which subsequently induce a cascade of anti-inflammatory cytokines and stunt pro-inflammatory T cell subsets [10,36,37]. This type of cell-cell communication acts through an “engulfment synapse” structure on the lipid raft [38], a model proposed to explain the tight coupling between the exposed PS on apoptotic cells, and the PS receptor TIM family and scavenger receptors including CD36 and LFA-1 on phagocytes [38–40]. Since TIM-3 is preferentially expressed on Th1 and Th17 cells [22], interaction with apoVs is not an exclusive privilege for phagocytes, and may be achieved in ways other than engulfment. Previous studies showed elevated level of TIM-3 on activated memory T cells in inflamed conditions such as lupus and arthritis over unstimulated naïve T cells, supporting our findings and making apoVs suitable for treating inflammatory disorders [41–43]. Furthermore, we observed restored TCR signaling and higher disease activity in T cells cocultured with A5-pretreated apoVs, suggesting the blockage of PS recognition promoted inflammatory phenotypes of T cells and aggravated autoimmune disorders [44]. From the perspective of T cells, our findings contribute to explaining the associations between defective apoptosis clearance and autoimmunity. While PS-mediated direct contact with T cells may account for the T cell suppressive effect of apoVs in large doses, there are clear evidence of other bioactive components in the apoVs which could be released into the circulation (Fig. 4H and I), and possibly components modulating other immune function and maintaining homeostasis (Fig. S3). Our recent work identified a plethora of proteins enriched in the KEGG immune system pathways within MSC-derived apoVs [12], and the specific bioactivities of these proteins,

as well as other components such as lipids and miRNAs in the apoVs, warrants further investigation in health and disease. These intriguing effects of apoVs call for future studies to explore their full potential in bioengineering and as therapies for other diseases.

There are several unanswered questions awaiting future investigation. First, although by replenishing apoVs we restored the apoV/T cell ratio in apoptosis-defective mice, the function of cell-specific apoVs in the local microenvironment remains to be elucidated. Second, the effect of apoVs on other immune cells is not fully explained. The conserved and common membrane interaction based on PS and its receptors indicates this mechanism can be exploited by many leukocytes including $CD8^+$ T cells, B cells, and myeloid cells in various scenarios. The therapeutic benefits of apoVs can be potentially applied in diseases featuring the dysregulation of these cells. For instance, apoVs may inhibit proximal TCR signaling via direct contact with T cells in $CD8^+$ T cells, and it may potentially alter anti-tumor immunity in the tumor microenvironment, while blocking PS recognition through A5 and TIM-3 blocking antibodies may provide therapeutic benefits. Lastly, based on the partial but not complete loss of suppressive capacity we observed with apoV-conditioned medium, there must be more functional molecules released into the medium. A broader profiling of the content in apoVs will therefore be important for more precise therapeutic application in the future.

4. Materials and methods

4.1. Mice

MRL/*lpr* (JAX #000485), MRL/MpJ (JAX #000486), C57BL/6 (JAX #000664), CD11b-DTR (JAX #006000) and DBA/1 (JAX #000670) mouse strains were obtained from Jackson Laboratory. Age-matched female MRL/*lpr* and MRL/MpJ mice were used at indicated ages for respective experiments. Both sexes of C57BL/6 and CD11b-DTR mice at ages of 8–12 weeks were used for respective experiments. Male DBA/1 mice at ages of 8–12 weeks were used for the collagen-induced arthritis model. All animal experiments were performed under animal research guidelines and an institutionally approved protocol at the University of Pennsylvania (IACUC #805478).

4.2. Culture of mouse BMMSCs

Mouse bone marrow-derived cells were isolated from limbs of C57BL/6 mice and adherent cells were maintained for 2 passages to enrich for BMMSCs, as previously described [1,15]. Briefly, marrow cells were flushed out of long bones with PBS supplemented with 10% fetal bovine serum (FBS) and seeded at a density of 1.5×10^7 cells per 10 cm culture dish. Non-adherent cells were removed after 48 h and attached cells were maintained for 16 days in alpha-Minimum Essential Medium (α-MEM) (12571-048, Invitrogen, USA) supplemented with 20% FBS (100–106, Gemini Bio, USA), 2 mM L-glutamine (35050-061, Invitrogen, USA), 55 μM 2-mercaptoethanol (21985-023, Invitrogen, USA), 100 U/mL Penicillin-Streptomycin (15140122, Gibco, USA) and 10 nM dexamethasone (50-02-2, Sigma-Aldrich, USA). BMMSCs at the second passage were analyzed for surface markers by flow cytometry and used in apoptotic induction and co-culture experiments.

4.3. Preparation of apoVs

Cell-derived apoVs were isolated from apoptotic cells using a serial centrifugation protocol we previously established [15] with modifications. Apoptosis was induced through multiple approaches in this study. To induce both caspase-dependent and caspase-independent apoptosis, cells were treated with 1 μM STS (ALX-380-014, Enzo Life Sciences, USA) in serum-free medium for 16–24 h. To induce apoptosis via the extrinsic pathway, cells were treated with anti-mouse CD95/Fas antibody (152803, BioLegend, USA) at 5 μg/mL for 48 h to crosslink Fas during cell activation. Apoptotic cells were observed under light microscopy and verified by Annexin V/7AAD staining (559763, BD Pharmingen, USA). Apoptotic cells and the medium were collected and centrifuged for 10 min twice separately at 300 g and 2,000 g at 4 °C to remove cell debris pellets. The supernatant was filtered through 5-μm filters and centrifuged for 30 min at 16,000 g at 4 °C to obtain apoV pellets. ApoVs were resuspended in sterile PBS for subsequent characterization and applications. EVs from non-apoptotic cells were isolated using the same centrifugation protocol for comparison.

Circulating apoVs were isolated from blood using the above protocol and identified as Annexin V^+ $CD62P^-$, as previously reported [15]. Spleen-derived apoVs were isolated from the desired tissue using a mechanical and chemical digestion protocol followed by serial centrifugation. Briefly, the spleen was weighed, cut into pieces and digested with 40 μg/ml liberase TM (LIBTM-RO, Sigma-Aldrich, USA) on a shaker for 30 min at 37 °C, and spleen EVs were collected using the above protocol.

4.4. ApoV characterization

For quantification and size distribution measurement, apoVs were analyzed using nanoparticle tracking analysis (NTA) and further validated with reference beads and surface Annexin V staining through flow cytometry.

For NTA analysis, apoV pellets were diluted in PBS, measured using NanoSight NS300 (Malvern Panalytical, UK) and analyzed with NTA software (Malvern Panalytical, UK).

Images of apoVs were obtained by transmission electron microscopy (TEM). Briefly, apoV pellets were diluted in PBS and fixed with 1% glutaraldehyde (G5882, Sigma-Aldrich, USA) for 30 min at 4 °C, absorbed onto glow-discharged 300-mesh heavy-duty carbon-coated formvar copper grids (ProSciTech, Australia) for 5 min, and the excess liquid was blotted on filter papers. Grids were washed twice with distilled water and negatively stained with 2.5% uranyl acetate (22400, Electron Microscopy Sciences, USA). Wide-field images encompassing multiple vesicles were taken on a JEM-1200EX electron microscope (JEOL, Japan).

4.5. ApoV application

For apoV labeling, the lipophilic membrane dye PKH26 (PKH26PCL, Sigma-Aldrich, USA) was used according to the manufacturer's instructions to label apoVs in culture or trace infused apoVs *in vivo*. In order to detect the biodistribution of apoVs, we performed IVIS imaging analysis (PerKin Elmer). Briefly, PKH26 labelled apoEVs were injected intraperitoneally, then mice were sacrificed at 1 day, 3 days and 7 days, respectively, after treatment. The distribution for each sample in different organ was analyzed via IVIS scanning. For co-culture experiments, quantitated apoVs were diluted in sterile PBS and cultured together with immune cells. For Annexin V pre-treatment, 1×10 [7] apoVs were centrifuged into pellets at 4 °C and then resuspended in 1x Annexin V binding buffer (422201, BioLegend, USA) containing 10 μg/mL Annexin V (C916J65, Sigma-Aldrich, USA) at 37 °C for 30 min before centrifuging again for downstream application. For apoV conditioned medium containing soluble components, quantitated apoVs were diluted in cell culture medium and kept at 37 °C for 3 days before centrifuging again to remove apoVs, and the supernatant was used for downstream application. For *in vivo* infusion, quantitated apoVs were diluted in sterile PBS and injected intraperitoneally.

4.6. Exosome preparation

Exosomes were isolated from cultured non-apoptotic cells using previously published protocols [45]. Briefly, cells were cultured in exosome-depleted medium (complete medium depleted of FBS-derived exosomes by overnight centrifugation at 100,000 g) for 48 h. EVs

from culture supernatants of 1×10^6 MSCs were isolated by differential centrifugation at 300*g* for 10 min, 3000 g for 10 min, 20,000 g for 30 min, and 120,000 g for 120 min.

4.7. Liposome preparation

Phosphatidylserine (PS, 840035P, Avanti Polar Lipids, USA) liposomes were prepared as previously described [46]. Briefly, 200 nm unilamellar vesicles of complete PS were made by extrusion. The lipid was dried by evaporation, then hydrated with sterile PBS for >30 min while kept at room temperature (above the phase transition temperature of the lipid). The hydrated lipid suspension was alternately placed in liquid nitrogen and a 37 °C water bath for 3 freeze/thaw cycles. The fully hydrated lipid was loaded into a gas-tight syringe and placed into one end of a Mini-Extruder (610000, Avanti Polar Lipids, USA). Another empty gas-tight syringe was placed into the other end of the Mini-Extruder. The extruder apparatus was then assembled with a pre-wetted 200 nm membrane (610006, Avanti Polar Lipids, USA) in the middle. The plungers of syringes were gently pushed 10 times for the entire volume of lipid to pass through the membrane completely each time. When the final extrusion filled the alternate syringe, the filled syringe was removed from the extruder and the lipid solution was injected into a clean sample vial. Liposomes were subjected to subsequent flow cytometry characterization and applications similar to apoVs.

4.8. Spontaneous lymphoproliferation and lupus in mice

MRL/*lpr* mice were monitored from 6 weeks of age for signs of lymphoproliferation, such as enlarged lymph nodes, and signs of autoimmunity, such as skin rash and proteinuria. Urine protein was measured twice a week using Fisherbrand urine reagent strips (23-111-262, Fisher Scientific, USA). Systemic administration of STS was given intraperitoneally, 3 ng twice a week for 4 weeks. Systemic administrations of apoVs derived from 1×10 [6] BMMSCs with or without annexin V pretreatment or PBS were given intraperitoneally once a week for 4 weeks or life-long based on the study design. At the time of harvest, mice were sacrificed rapidly and humanely, followed by rapid isolation of the blood, spleen, lymph nodes and kidney for downstream analysis.

4.9. Induced CD11b depletion in CD11b-DTR mice

100 ng of diphtheria toxin (322326, Sigma-Aldrich, USA) in PBS was injected intraperitoneally on day 0 to deplete $CD11b^+$ cells. To assess the role of $CD11b^+$ macrophages, apoVs were administered on day 2 after verifying the depletion efficiency and mice were harvested on day 3.

4.10. Collagen-induced arthritis

Inflammatory arthritis was induced in male DBA/1 mice with type II collagen, as previously described [47]. In brief, a primary immunization was performed on day 0 with a subcutaneous injection (at the base of the tail) of 100 μL (per mouse) emulsion containing 100 μg type II collagen (20012, Chondrex.Inc, USA) and complete Freud adjuvant (7009, Chondrex.Inc, USA), followed by a booster immunization with 100 μL (per mouse) emulsion containing 100 μg type II collagen and incomplete Freud adjuvant on day 7 or day 21. Systemic administration of EVs derived from 1×10 [6] BMMSCs with or without annexin V pretreatment, an equivalent number of PS liposomes, 1×10 [6] BMMSCs, 50 μg/20 g body weight TNF neutralizing antibody (506332, BioLegend, USA) or PBS was performed at indicated time points based on the study design. Arthritic symptoms and the general condition of mice were assessed daily. For assessing the severity of arthritis, clinical symptoms were evaluated on a five-point scale: 0 = no damage; 1 = detectable swelling in a single digit; 2 = swelling of more than one digit; 3 = swelling of multiple digits and the paw; and 4 = severe swelling of the paw and the ankle or apparent deformity. At the endpoint of the experiments, mice were sacrificed rapidly and humanely, followed by rapid isolation of the blood, limbs and joints, spleen and draining lymph nodes for downstream analysis.

4.11. Culture of mouse splenocytes and T lymphocytes

Splenocytes were isolated from mouse spleen by grinding up the desired spleen tissue with a sterile plunger and passing through a 70 nm strainer. ACK lysis buffer (10-548E, Lonza Bioscience, Switzerland) was used to lyse red blood cells. Total $CD4^+$ T cells and naïve $CD25^-CD4^+$ T cells were isolated from mouse spleen using magnetic beads (130-091-041, Miltenyi Biotec, Germany). Splenocytes and T cells were cultured in RPMI 1640 medium (12-702Q, Lonza Bioscience, Switzerland) supplemented with 10% FBS (17L624, Sigma-Aldrich, USA), 55 μM 2-mercaptoethanol, 10 mM HEPES (BE17-737E, Lonza Bioscience, Switzerland), Non-Essential Amino Acids (11140050, Gibco, USA), 1 mM sodium pyruvate (11360070, Gibco, USA) and 100 U/mL Penicillin-Streptomycin (15140122, Gibco, USA). T cells were stimulated in culture with plate-bound anti-mouse CD3 antibody (100340, BioLegend, USA) and soluble anti-mouse CD28 antibody (102116, BioLegend, USA) both at 2 μg/ml if not otherwise specified.

4.12. Th17 differentiation

Naïve $CD25^-CD4^+$ T cells were stimulated with anti-CD3/CD28 antibody under Th17 polarization conditions for 3 days with IL-6 (50 ng/mL, R&D Systems, USA), human TGF-β1 (2 ng/mL, R&D Systems, USA), anti-IFN-γ neutralizing antibodies (10 μg/mL, Biolegend, USA) and anti-IL-4 neutralizing antibodies (10 μg/mL, Biolegend, USA).

4.13. Human PBMC culture

Human PBMCs were obtained from healthy blood donors with informed consent at Renji hospital approved by institutionally ethics committee, and cultured with or without plate-bound anti-human CD3 antibody (300401, BioLegend, USA) and soluble anti-human CD28 antibody (302901, BioLegend, USA) each at 2 μg/ml.

4.14. Flow cytometry

The following antibodies and reagents were used for flow cytometric phenotyping: anti-mouse CD3 (clone 17A2), CD4-PerCP/Cy5.5 (clone GK1.5), CD25-APC (clone 3C7), CD44-PE (clone IM7), CD62L (clone MEL-14), Sca-1 (clone E13–161.7), CD105 (clone MJ7/18), CD29 (clone HMβ1-1), CD34 (clone HM34), CD45 (clone 30-F11), IFN-γ (clone XMG1.2), IL-4 (clone 11B11), IL-17A (clone TC11-18H10.1), and Foxp3 (clone MF-14); anti-human CD3 (clone UCHT1), CD4 (clone OKT4), CD25 (clone M-A251), and the intracellular staining permeabilization wash buffer (421002) were purchased from BioLegend, USA. The eBioscience Fixation/Permeabilization concentrate and diluent kit (00-5521-00) was purchased from Thermo Fisher Scientific, USA. Samples were acquired using a FACS Calibur Flow Cytometer (BD Biosciences, USA). Data were analyzed using FlowJo v10 software (FlowJo LLC, USA).

4.15. Enzyme-linked immunosorbent assay (ELISA)

The following reagents were used according to the manufacturer's instructions for detection in serum and culture supernatants: IL-2 (431001), IFN-γ (430801), IL-10 (431411), and IL-17A (432501). ELISA kits were obtained from BioLegend, USA. Autoantibody detection kits for ANA (5210) and anti-dsDNA IgG (5120) were obtained from Alpha Diagnostic International, USA.

4.16. Western blotting

The following antibodies and reagents were used for western blotting: RIPA Lysis Buffer System with protease and phosphatase inhibitors (sc-24948, Santa Cruz Biotechnology, USA); UltraRIPA kit for lipid raft (F015, Diagnocine, Japan); Pierce™ BCA Protein Assay Kit (23225, Thermo Scientific, USA). Anti-mouse antibodies included p-CD3 (67748S), p-ZAP70 (2717T), p-LCK (2751T), p-PLCγ (14008S), NFAT1 (5861), and Tim-3 (83882), Caveolin-1 (3267) from Cell Signaling Technology, USA. Anti-mouse β-Actin antibody (A5441) was from Sigma-Aldrich, USA. Protein was extracted from cultured cells and quantified to obtain comparable loading amounts. A total of 20 μg protein per sample was loaded onto 4%–12% NuPAGE gel (NP0321BOX/NP0322BOX, Invitrogen, USA) for electrophoresis and was transferred to 0.2 μm methanol-activated nitrocellulose membranes (Millipore, USA). Membranes with protein were then blocked with 5% bovine serum albumin (BSA) (700-100P, Gemini Bio, USA) at room temperature for 1 h, followed by primary antibody incubation overnight at 4 °C and 1 h room temperature incubation with horseradish peroxidase (HRP)-conjugated secondary antibodies (sc-516102/sc-2357, Santa Cruz Biotechnology, USA; or 7077, Cell Signaling Technology, USA) with sufficient washing between incubations. Signal was detected using SuperSignal™ West Pico PLUS Chemiluminescent Substrate (34580, Thermo Scientific, USA), SuperSignal™ West Femto Maximum Sensitivity Substrate (34095, Thermo Scientific, USA), and ChemiDoc MP Imaging System (Bio-Rad, USA).

4.17. Tissue histology

At the time of harvest, tissues were rapidly isolated and fixed overnight with 4% paraformaldehyde (PFA) (150146, MP Biomedicals, USA). Hard tissues such as joint and bone were decalcified with 10% EDTA. For histological analyses, samples were either dehydrated and embedded in paraffin or cryopreserved with optimal cutting temperature (OCT) compound (4583, Sakura Finetek, USA). 5–10 μm serial sections were prepared (RM2125, Leica, Germany). Sections then underwent either hematoxylin and eosin (H&E) staining, Masson's trichrome staining (HT15-1 KT, Sigma-Aldrich, USA) staining or Sirius red/fast green staining (9046, Chondrex.Inc, USA) following the manufacturer's instructions; or underwent immunofluorescence staining, as detailed below.

4.18. Immunofluorescence

The following antibodies and reagents were used for immunofluorescence (IF) detection of T cells and live cell imaging: Cholera Toxin B subunit for GM-1/lipid raft staining (C1655, Sigma-Aldrich, USA), anti-mouse CD3 (APA1/1, 362701, BioLegend, USA) and Tim-3 (83882, Cell Signaling Technology, USA), Triton X-100 (X100-100 ML, Sigma-Aldrich, USA), mounting medium with DAPI (ab104139, Abcam, UK), and Nunc coverslip (174977, Thermo Fisher Scientific, USA). For IF staining of infiltrating T cells in tissues, cryopreserved tissues were used. For IF staining of cultured cells and live cell imaging, cells with or without co-cultured PKH26-labelled EVs were seeded on coverslips then fixed with 4% PFA at the time of collection. Tissue sections or coverslips were blocked with 5% BSA for 1 h at room temperature, then stained with primary antibodies overnight at 4 °C, then washed and stained with appropriate secondary antibodies (Alexa Fluor 488-conjugated goat anti-mouse secondary antibody, A-11001; Alexa Fluor 647-conjugated goat anti-rat secondary antibody, A-21247; or Alexa Fluor 647-conjugated goat anti-rabbit secondary antibody A-21245, Invitrogen, USA) for 1 h at room temperature, then washed and counterstained by DAPI.

4.19. Image acquisition and analyses

Bright-field images were obtained using an inverted microscope (Axio Observer 5, Zeiss, Germany). Fluorescent images were obtained using confocal microscopes (SP5-II, Leica, Germany; or LSM 900, Zeiss, Germany). Imaging analysis was performed with ImageJ 1.47 software (National Institutes of Health, USA).

4.20. Arthritis histological score

Based on H&E staining and Sirius/fast green staining of joints, an arthritis histological score with a maximum of 15 points was calculated by grading three separate aspects: (a) inflammation of the affected joint, the synovium and the surrounding tissue: 0-normal, 1-a few infiltrating immune cells, 2-mild infiltration, 3-moderate infiltration and edema, 4-apparent infiltration and edema at multiple loci, 5-diffused and severe infiltration and edema; (b) pannus formation: 0-normal tissue without pannus, 1-mild pannus formation and damage to the superficial layer of cartilage, 2-mild pannus extending into the subchondral bone with mild erosion of the bone cortex, 3-moderate pannus extension with moderate damages to the joint hard tissue, 4-severe pannus extension with obvious damages to the joint structure involving multiple joints, 5- severe pannus extension with complete joint destruction; (c) erosion of bone and cartilage: 0-normal tissue without erosion, 1-mild erosion involving small area of cartilage or bone cortex without obvious damage to cartilage or bone collagen with low magnification (10x), 2-mild erosion of bone cortex and medulla and increased erosion area with visible damage to cartilage or bone, 3-moderate erosion of bone cortex and medulla without complete disruption at multiple loci, 4-severe erosion and distortion of bone cortex and medulla involving multiple joints, 5-severe erosion and complete disruption of bone cortex and joint destruction [48,49].

4.21. Micro CT

4% PFA-fixed joints were imaged and analyzed using a high-resolution Scanco μCT35 scanner (Scanco Medical AG, Bruttisellen, Switzerland). The specimens were scanned using an isotropic voxel size of 10 μm at 160 μA, with 250 projections, a photon energy of 50 keV, and integration time of 300 msec. Scanned data were reconstructed using Scanco software. Datasets were loaded into Amira 5.3.1 software (Visage Imaging, Berlin, Germany) for visualization and analysis. Bone mineral density (BMD) and bone volume/total volume (BV/TV) for each specimen were also calculated using the Amira software. A radiographic visual scoring system previously described was used to evaluate the severity of arthritis [50]. Briefly, individual joins including the metatarsophalangeal joints (MTP), metacarpophalangeal joints (MCP), distal and proximal interphalangeal joints (DIP and PIP), except the first DIP joints, were evaluated for the degree of erosions and periarticular osteoporosis with a 6-point score, ranging from 0 (normal) to 5 (severe).

4.22. Statistical analyses

Data were represented as the mean ± standard deviation (SD) unless otherwise indicated. Statistical significance was evaluated using Prism 8 software (GraphPad, USA). We performed Shapiro-Wilk normality test (alpha 0.05) to determine the distribution of data. Mann-Whitney test for two-group comparisons and Kruskal-Wallis test for multiple comparisons were used for non-normally distributed data. Two-tailed Student's *t*-test for two-group comparisons, by one-way analysis of variation (ANOVA) followed by the Holm-Sidak test for multiple comparisons for normally distributed data. Logrank Mantel-Cox test with area under curve was calculated for curve comparisons. A p value < 0.05 was considered as statistically significant.

Ethics approval and consent to participate

All animal experiments were performed under animal research guidelines and an institutionally approved protocol at the University of

Pennsylvania (IACUC #805478).

Human PBMCs were obtained from healthy blood donors with informed consent at Renji hospital approved by institutionally ethics committee.

Data availability

All data generated during and analyzed during the current study are included in this published article (and its supplementary information files), and available from the corresponding author on reasonable request.

CRediT authorship contribution statement

Runci Wang: Conceptualization, Data curation, Formal analysis, Funding acquisition, Investigation, Methodology, Resources, Visualization, Writing – original draft, Writing – review & editing. **Meng Hao:** Data curation, Formal analysis, Investigation, Validation, Visualization, Writing – original draft, Writing – review & editing. **Xiaoxing Kou:** Funding acquisition, Investigation, Methodology, Writing – review & editing. **Bingdong Sui:** Investigation, Methodology. **Maria Laura Sanmillan:** Data curation, Formal analysis, Investigation. **Xiao Zhang:** Investigation, Methodology. **Dawei Liu:** Investigation, Methodology. **Jun Tian:** Investigation. **Wenjing Yu:** Investigation. **Chider Chen:** Investigation. **Ruili Yang:** Investigation. **Lingyun Sun:** Investigation, Writing – review & editing. **Yi Liu:** Investigation, Writing – review & editing. **Claudio Giraudo:** Data curation, Formal analysis, Investigation. **Deepak A. Rao:** Investigation, Writing – review & editing. **Nan Shen:** Investigation, Writing – review & editing. **Songtao Shi:** Conceptualization, Formal analysis, Funding acquisition, Investigation, Methodology, Project administration, Resources, Supervision, Writing – review & editing.

Declaration of competing interest

The authors declare no conflict of interests.

Acknowledgement

This work was supported by grants from the State Scholarship Fund of China (201506240225to R.W.), the Pearl River Talent Recruitment Program (2019ZT08Y485, 2019QN01Y138, 2019JC01Y182), the National Key R&D Program of China (2021YFA1100600to S.S.), the Guangdong Financial Fund for High-Caliber Hospital Construction (174-2018-XMZC-0001-03-0125, D-07 to S.S., C-03 and D-11 to X.K.), and the National Natural Science Foundation of China (82170924to X.K.). We sincerely appreciate Drs. Chun Liu and Tobias Baumgart at the Department of Chemistry, School of Arts & Sciences, University of Pennsylvania for their expert advice and experimental help with liposome preparation. We thank Dr. Yongchun Gu for sharing his experience on collagen-induced arthritis.

Appendix A. Supplementary data

Supplementary data to this article can be found online at https://doi.org/10.1016/j.bioactmat.2022.07.026.

References

[1] K. Akiyama, et al., Mesenchymal-stem-cell-induced immunoregulation involves FAS-ligand-/FAS-mediated T cell apoptosis, Cell Stem Cell 10 (2012) 544–555, https://doi.org/10.1016/j.stem.2012.03.007.

[2] M. Xie, et al., Immunoregulatory effects of stem cell-derived extracellular vesicles on immune cells, Front. Immunol. 11 (2020) 13, https://doi.org/10.3389/fimmu.2020.00013.

[3] R. Roozendaal, R.E. Mebius, Stromal cell-immune cell interactions, Annu. Rev. Immunol. 29 (2011) 23–43, https://doi.org/10.1146/annurev-immunol-031210-101357.

[4] D. Wang, et al., A long-term follow-up study of allogeneic mesenchymal stem/stromal cell transplantation in patients with drug-resistant systemic lupus erythematosus, Stem Cell Rep. 10 (2018) 933–941, https://doi.org/10.1016/j.stemcr.2018.01.029.

[5] J.M. Alvaro-Gracia, et al., Intravenous administration of expanded allogeneic adipose-derived mesenchymal stem cells in refractory rheumatoid arthritis (Cx611): results of a multicentre, dose escalation, randomised, single-blind, placebo-controlled phase Ib/IIa clinical trial, Ann. Rheum. Dis. 76 (2017) 196–202, https://doi.org/10.1136/annrheumdis-2015-208918.

[6] N. Luque-Campos, et al., Mesenchymal stem cells improve rheumatoid arthritis progression by controlling memory T cell response, Front. Immunol. 10 (2019) 798, https://doi.org/10.3389/fimmu.2019.00798.

[7] S. Aggarwal, M.F. Pittenger, Human mesenchymal stem cells modulate allogeneic immune cell responses, Blood 105 (2005) 1815–1822, https://doi.org/10.1182/blood-2004-04-1559.

[8] L. von Bahr, et al., Analysis of tissues following mesenchymal stromal cell therapy in humans indicates limited long-term engraftment and no ectopic tissue formation, Stem Cell. 30 (2012) 1575–1578, https://doi.org/10.1002/stem.1118.

[9] K. Kallmeyer, et al., Fate of systemically and locally administered adipose-derived mesenchymal stromal cells and their effect on wound healing, Stem Cells Transl Med 9 (2020) 131–144, https://doi.org/10.1002/sctm.19-0091.

[10] A. Galleu, et al., Apoptosis in mesenchymal stromal cells induces in vivo recipient-mediated immunomodulation, Sci. Transl. Med. 9 (2017), https://doi.org/10.1126/scitranslmed.aam7828.

[11] Y. Shi, et al., Immunoregulatory mechanisms of mesenchymal stem and stromal cells in inflammatory diseases, Nat. Rev. Nephrol. 14 (2018) 493–507, https://doi.org/10.1038/s41581-018-0023-5.

[12] X. Zhang, et al., Proteomic analysis of MSC-derived apoptotic vesicles identifies Fas inheritance to ameliorate haemophilia a via activating platelet functions, J. Extracell. Vesicles 11 (2022), e12240, https://doi.org/10.1002/jev2.12240.

[13] L. Ma, et al., Apoptotic extracellular vesicles are metabolized regulators nurturing the skin and hair, Bioact. Mater. 19 (2023) 626–641, https://doi.org/10.1016/j.bioactmat.2022.04.022.

[14] O.P.B. Wiklander, M.A. Brennan, J. Lotvall, X.O. Breakefield, S. El Andaloussi, Advances in therapeutic applications of extracellular vesicles, Sci. Transl. Med. 11 (2019), https://doi.org/10.1126/scitranslmed.aav8521.

[15] D. Liu, et al., Circulating apoptotic bodies maintain mesenchymal stem cell homeostasis and ameliorate osteopenia via transferring multiple cellular factors, Cell Res. 28 (2018) 918–933, https://doi.org/10.1038/s41422-018-0070-2.

[16] C. Zheng, et al., Apoptotic vesicles restore liver macrophage homeostasis to counteract type 2 diabetes, J. Extracell. Vesicles 10 (2021), e12109, https://doi.org/10.1002/jev2.12109.

[17] Q. Ou, et al., Electrostatic charge-mediated apoptotic vesicle biodistribution attenuates sepsis by switching neutrophil NETosis to apoptosis, Small 18 (2022), e2200306, https://doi.org/10.1002/smll.202200306.

[18] X.C. Li, T.B. Strom, L.A. Turka, A.D. Wells, T cell death and transplantation tolerance, Immunity 14 (2001) 407–416, https://doi.org/10.1016/s1074-7613(01)00121-2.

[19] M.C. Bittencourt, et al., Intravenous injection of apoptotic leukocytes enhances bone marrow engraftment across major histocompatibility barriers, Blood 98 (2001) 224–230, https://doi.org/10.1182/blood.v98.1.224.

[20] N. Karbian, et al., Apoptotic cell therapy for cytokine storm associated with acute severe sepsis, Cell Death Dis. 11 (2020) 535, https://doi.org/10.1038/s41419-020-02748-8.

[21] M. Nicolier, A.Z. Decrion-Barthod, S. Launay, J.L. Pretet, C. Mougin, Spatiotemporal activation of caspase-dependent and -independent pathways in staurosporine-induced apoptosis of p53wt and p53mt human cervical carcinoma cells, Biol. Cell. 101 (2009) 455–467, https://doi.org/10.1042/BC20080164.

[22] G.J. Freeman, J.M. Casasnovas, D.T. Umetsu, R.H. DeKruyff, TIM genes: a family of cell surface phosphatidylserine receptors that regulate innate and adaptive immunity, Immunol. Rev. 235 (2010) 172–189, https://doi.org/10.1111/j.0105-2896.2010.00903.x.

[23] J. Leipe, et al., Role of Th17 cells in human autoimmune arthritis, Arthritis Rheum. 62 (2010) 2876–2885, https://doi.org/10.1002/art.27622.

[24] Y. Gu, S. Shi, Transplantation of gingiva-derived mesenchymal stem cells ameliorates collagen-induced arthritis, Arthritis Res. Ther. 18 (2016) 262, https://doi.org/10.1186/s13075-016-1160-5.

[25] K. Le Blanc, et al., Treatment of severe acute graft-versus-host disease with third party haploidentical mesenchymal stem cells, Lancet 363 (2004) 1439–1441, https://doi.org/10.1016/S0140-6736(04)16104-7.

[26] L. Kordelas, et al., MSC-derived exosomes: a novel tool to treat therapy-refractory graft-versus-host disease, Leukemia 28 (2014) 970–973, https://doi.org/10.1038/leu.2014.41.

[27] I.L. Colao, R. Corteling, D. Bracewell, I. Wall, Manufacturing exosomes: a promising therapeutic platform, Trends Mol. Med. 24 (2018) 242–256, https://doi.org/10.1016/j.molmed.2018.01.006.

[28] J.Q. Yin, J. Zhu, J.A. Ankrum, Manufacturing of primed mesenchymal stromal cells for therapy, Nat. Biomed. Eng. 3 (2019) 90–104, https://doi.org/10.1038/s41551-018-0325-8.

[29] I. Hwang, X. Shen, J. Sprent, Direct stimulation of naive T cells by membrane vesicles from antigen-presenting cells: distinct roles for CD54 and B7 molecules, Proc. Natl. Acad. Sci. U. S. A. 100 (2003) 6670–6675, https://doi.org/10.1073/pnas.1131852100.

[30] S. Datta, N. Sarvetnick, Lymphocyte proliferation in immune-mediated diseases, Trends Immunol. 30 (2009) 430–438, https://doi.org/10.1016/j.it.2009.06.002.

[31] A.M. Gizinski, D.A. Fox, T cell subsets and their role in the pathogenesis of rheumatic disease, Curr. Opin. Rheumatol. 26 (2014) 204–210, https://doi.org/10.1097/BOR.0000000000000036.
[32] V.R. Moulton, G.C. Tsokos, T cell signaling abnormalities contribute to aberrant immune cell function and autoimmunity, J. Clin. Invest. 125 (2015) 2220–2227, https://doi.org/10.1172/JCI78087.
[33] J.M. Pitt, G. Kroemer, L. Zitvogel, Immunogenic and non-immunogenic cell death in the tumor microenvironment, Adv. Exp. Med. Biol. 1036 (2017) 65–79, https://doi.org/10.1007/978-3-319-67577-0_5.
[34] P. Vanlandschoot, G. Leroux-Roels, Viral apoptotic mimicry: an immune evasion strategy developed by the hepatitis B virus? Trends Immunol. 24 (2003) 144–147, https://doi.org/10.1016/s1471-4906(03)00026-7.
[35] I.K. Poon, C.D. Lucas, A.G. Rossi, K.S. Ravichandran, Apoptotic cell clearance: basic biology and therapeutic potential, Nat. Rev. Immunol. 14 (2014) 166–180, https://doi.org/10.1038/nri3607.
[36] H. Kazama, et al., Induction of immunological tolerance by apoptotic cells requires caspase-dependent oxidation of high-mobility group box-1 protein, Immunity 29 (2008) 21–32, https://doi.org/10.1016/j.immuni.2008.05.013.
[37] A.G. N, et al., Apoptotic cells promote their own clearance and immune tolerance through activation of the nuclear receptor LXR, Immunity 31 (2009) 245–258, https://doi.org/10.1016/j.immuni.2009.06.018.
[38] C. Grimsley, K.S. Ravichandran, Cues for apoptotic cell engulfment: eat-me, don't eat-me and come-get-me signals, Trends Cell Biol. 13 (2003) 648–656, https://doi.org/10.1016/j.tcb.2003.10.004.
[39] K.S. Ravichandran, Find-me and eat-me signals in apoptotic cell clearance: progress and conundrums, J. Exp. Med. 207 (2010) 1807–1817, https://doi.org/10.1084/jem.20101157.
[40] K.S. Ravichandran, "Recruitment signals" from apoptotic cells: invitation to a quiet meal, Cell 113 (2003) 817–820, https://doi.org/10.1016/s0092-8674(03)00471-9.
[41] S. Mujib, et al., Antigen-independent induction of Tim-3 expression on human T cells by the common gamma-chain cytokines IL-2, IL-7, IL-15, and IL-21 is associated with proliferation and is dependent on the phosphoinositide 3-kinase pathway, J. Immunol. 188 (2012) 3745–3756, https://doi.org/10.4049/jimmunol.1102609.
[42] S. Li, et al., Expression of TIM-3 on CD4+ and CD8+ T cells in the peripheral blood and synovial fluid of rheumatoid arthritis, APMIS 122 (2014) 899–904, https://doi.org/10.1111/apm.12228.
[43] J.S. Tilstra, et al., Kidney-infiltrating T cells in murine lupus nephritis are metabolically and functionally exhausted, J. Clin. Invest. 128 (2018) 4884–4897, https://doi.org/10.1172/JCI120859.
[44] A. Bondanza, et al., Inhibition of phosphatidylserine recognition heightens the immunogenicity of irradiated lymphoma cells in vivo, J. Exp. Med. 200 (2004) 1157–1165, https://doi.org/10.1084/jem.20040327.
[45] C. Thery, S. Amigorena, G. Raposo, A. Clayton, Isolation and characterization of exosomes from cell culture supernatants and biological fluids, Curr. Protoc .Cell Biol. (2006), https://doi.org/10.1002/0471143030.cb0322s30. Chapter 3, Unit 3 22.
[46] F. Szoka Jr., D. Papahadjopoulos, Comparative properties and methods of preparation of lipid vesicles (liposomes), Annu. Rev. Biophys. Bioeng. 9 (1980) 467–508, https://doi.org/10.1146/annurev.bb.09.060180.002343.
[47] D.D. Brand, K.A. Latham, E.F. Rosloniec, Collagen-induced arthritis, Nat. Protoc. 2 (2007) 1269–1275, https://doi.org/10.1038/nprot.2007.173.
[48] K.W. McIntyre, et al., A highly selective inhibitor of I kappa B kinase, BMS-345541, blocks both joint inflammation and destruction in collagen-induced arthritis in mice, Arthritis Rheum. 48 (2003) 2652–2659, https://doi.org/10.1002/art.11131.
[49] P.F. Sumariwalla, et al., A novel synthetic, nonpsychoactive cannabinoid acid (HU-320) with antiinflammatory properties in murine collagen-induced arthritis, Arthritis Rheum. 50 (2004) 985–998, https://doi.org/10.1002/art.20050.
[50] K.H. Barck, et al., Quantification of cortical bone loss and repair for therapeutic evaluation in collagen-induced arthritis, by micro-computed tomography and automated image analysis, Arthritis Rheum. 50 (2004) 3377–3386, https://doi.org/10.1002/art.20557.